

A $\ell_2 - \ell_p$ regulariser based model for Poisson noise removal using augmented Lagrangian method

Abdul Halim¹, Abdur Rohim²

¹Department of Mathematics, Memari College, West Bengal, India
²Department of Mathematics, Raiganj University, West Bengal, India

November 20, 2024

1 Abstract

In this article, we propose a variational PDE model using $\ell_2 - \ell_p$ regulariser for removing Poisson noise in presence of blur. The proposed minimization problem is solved using augmented Lagrangian method. The convergence of the sequence of minimizers have been carried out. Numerical simulations on some standard test images have been shown. The numerical results are compared with that of a few models existed in literature in terms of image quality metric such as SSIM, PSNR and SNR.

Keywords: Poisson Noise removal, Variational PDE, Augmented Lagrangian Method, Image denoising.

2 Introduction

Denoising of a noisy image is an important task in the area of image processing. During the image acquisition, transmission several noises like Gaussian noise, Poisson noise and Gamma noise may occurs in the image. Most of the models dealing with denoising is for removing Gaussian type of noise [1, 2, 3, 4, 5]. There are very few models to denoise Poisson [6, 13, 18] and Gamma noise [15]. In this paper we will focus on Poisson noise removal in presence of blur using PDE based model. The Poisson noise appear is medical images and astronomical images.

The first variational PDE based model for removing Poisson noise is proposed by Le, Chartrand, and Asaki in 2007 [6]. They have modified the fidelity term of ROF model [2], used for Gaussian noise removal. They have proposed the following model:

$$\min_u \left\{ \int_{\Omega} |\nabla u| dx + \lambda \int_{\Omega} (u - f \log u) dx \right\} \quad (2.1)$$

where f is the given noisy image and Ω is the domain of the image in \mathbb{R}^2 and λ is a positive constant called the fidelity parameter and u is the true image that has to be recover. The corresponding PDE model is solved using the classical bruit-force method.

Further, the researchers have proposed several models [7, 8] for denoising images with Poisson noise in presence of blur using the following modified model:

$$\min_u \left\{ \int_{\Omega} |\nabla u| dx + \lambda \int_{\Omega} (\mathcal{A}u - f \log \mathcal{A}u) dx \right\} \quad (2.2)$$

where \mathcal{A} is the blur operator. In [7, 8], the minimization problems were solved directly using split Bregman technique proposed in [9]. The total variational based models gives preserve edges but it suffer from stair case effect. To overcome the effect few models have been proposed like total generalised variation based model [10, 11], fractional-order TV model [12].

Another effective model for removing Gaussian noise was successfully implemented in [14]. They have used a convex variant of Mumford-shah model [19]. They have solve the following model:

$$\min \frac{\mu}{2} \int_{\Omega} |\nabla u|^2 dx + \int_{\Omega} |\nabla u| + \frac{\lambda}{2} \int_{\Omega} (f - \mathcal{A}u)^2 dx \quad (2.3)$$

We termed this model as $\ell_2 - \ell_1$ model in the rest of the paper. Further the model (2.3) is used for denoising images with Poisson noise and Gamma noise, by modifying the fidelity term in [15]. These models are quite good for noise removing and preserving edges. But these models suffer from the stair case effect [16]. To overcome the staircase effect Wu et.al. [16] have proposed a model for effecting Gaussian noise removal and segmentation. They have proposed a model using $\ell_2 - \ell_p$ regularisation. Their model is as follows:

$$\min \frac{\mu}{2} \int_{\Omega} |\nabla u|^2 dx + \int_{\Omega} |\nabla u|^p + \frac{\lambda}{2} \int_{\Omega} (f - \mathcal{A}u)^2 dx \quad (2.4)$$

where $p \in [0, 1]$. Note that if $p = 1$, the model (2.4) takes the form of model (2.3). Note that these models are actually proposed for image segmentation which is done in two stage. The first stage is nothing but denoising of images with blur. In this paper, we use a variant of $\ell_2 - \ell_p$ model for Poission noise removal with blur. Actually, the fidelity term of the model (2.3) has to replaced by a suitable fidelity term effective for Poission noise removal. The proposed model is solved using the augmented Lagrangian method .

The paper is organised as follows. In Section 3, we will discuss our proposed model and augmented Lagrangian method for the proposed model. The convergence analysis will be carried out in Section 4. The numerical results on some standard test images reported and analysed in section 5. Finally we draw some conclusion in section 6 based on the numerical results obtained by the experiment.

3 Proposed Model

We propose the following model for removing Poisson noise:

$$\min \frac{\mu}{2} \int_{\Omega} |\nabla u|^2 dx + \int_{\Omega} |\nabla u|^p + \lambda \int_{\Omega} (\mathcal{A}u - f \log \mathcal{A}u) dx \quad (3.1)$$

where \mathcal{A} is a non-negative linear operator which represents the blur and f is the given noisy image. We call this model as $l_2 - l_p$ model for Poission noise removal. Now

$$\min \left\{ \frac{\mu}{2} \|\nabla u\|_2^2 + \|(v, w)\|_p^p + \lambda \int_{\Omega} (z - f \log z) dz \right\} \quad (3.2)$$

where $v = \nabla_x u$, $w = \nabla_y u$, $z = \mathcal{A}u$. We solve the proposed by the augmented Lagrangian method as [17]. To solve (3.1), let us define the function often called as augmented Lagrangian function as:

$$\begin{aligned} \mathcal{L}(u, v, w, z, \lambda_1, \lambda_2, \lambda_3) = & \frac{\mu}{2} \|\nabla u\|_2^2 + \|(v, w)\|_p^p + \lambda \langle 1, z - f \log z \rangle - \langle \lambda_1, v - \nabla_x u \rangle \\ & + \frac{\gamma_1}{2} \|v - \nabla_x u\|_2^2 - \langle \lambda_2, w - \nabla_y u \rangle + \frac{\gamma_2}{2} \|w - \nabla_y u\|_2^2 \\ & - \langle \lambda_3, z - \mathcal{A}u \rangle + \frac{\gamma_3}{2} \|z - \mathcal{A}u\|_2^2 \end{aligned} \quad (3.3)$$

with Lagrangian multipliers $\lambda_1, \lambda_2, \lambda_3$ and positive parameters $\gamma_1, \gamma_2, \gamma_3$.

Finding the solution of (3.1) is same as to find a saddle point $(u^*, v^*, w^*, z^*, \lambda_1^*, \lambda_2^*, \lambda_3^*)$ of $\mathcal{L}(u, v, w, z, \lambda_1, \lambda_2, \lambda_3)$ satisfying

$$\mathcal{L}(u^*, v^*, w^*, z^*, \lambda_1, \lambda_2, \lambda_3) \leq \mathcal{L}(u^*, v^*, w^*, z^*, \lambda_1^*, \lambda_2^*, \lambda_3^*) \leq \mathcal{L}(u, v, w, z, \lambda_1^*, \lambda_2^*, \lambda_3^*) \quad (3.4)$$

The problem (3.4) can be reformulate as

$$\begin{aligned} (u^{k+1}, v^{k+1}, w^{k+1}, z^{k+1}) = \underset{u, v, w, z}{\operatorname{argmin}} & \frac{\mu}{2} \|\nabla u\|_2^2 + \|(v, w)\|_p^p + \lambda \langle 1, z - f \log z \rangle - \langle \lambda_1^k, v - \nabla_x u \rangle \\ & + \frac{\gamma_1}{2} \|v - \nabla_x u\|_2^2 - \langle \lambda_2^k, w - \nabla_y u \rangle + \frac{\gamma_2}{2} \|w - \nabla_y u\|_2^2 - \langle \lambda_3^k, z - \mathcal{A}u \rangle + \frac{\gamma_3}{2} \|z - \mathcal{A}u\|_2^2 \end{aligned} \quad (3.5)$$

where the formulas for updated $\lambda_1^{k+1}, \lambda_2^{k+1}, \lambda_3^{k+1}$

$$\begin{aligned} \lambda_1^{k+1} &= \lambda_1^k + \gamma_1 (\nabla_x u^{k+1} - v^{k+1}) \\ \lambda_2^{k+1} &= \lambda_2^k + \gamma_2 (\nabla_y u^{k+1} - w^{k+1}) \\ \lambda_3^{k+1} &= \lambda_3^k + \gamma_3 (\mathcal{A}u^{k+1} - z^{k+1}) \end{aligned} \quad (3.6)$$

The optimization problem (3.5) can be decomposed into three sub-problems

$$\begin{aligned} u^{k+1} &= \underset{u}{\operatorname{argmin}} \left\{ \frac{\mu}{2} \|\nabla u\|_2^2 - \langle \lambda_1^k, v^k - \nabla_x u \rangle + \frac{\gamma_1}{2} \|v^k - \nabla_x u\|_2^2 - \langle \lambda_2^k, w^k - \nabla_y u \rangle \right. \\ & \quad \left. + \frac{\gamma_2}{2} \|w^k - \nabla_y u\|_2^2 - \langle \lambda_3^k, z^k - \mathcal{A}u \rangle + \frac{\gamma_3}{2} \|z^k - \mathcal{A}u\|_2^2 \right\} \\ (v^{k+1}, w^{k+1}) &= \underset{v, w}{\operatorname{argmin}} \left\{ \|(v, w)\|_p^p - \langle \lambda_1^k, v - \nabla_x u^{k+1} \rangle + \frac{\gamma_1}{2} \|v - \nabla_x u^{k+1}\|_2^2 \right. \\ & \quad \left. - \langle \lambda_2^k, w - \nabla_y u^{k+1} \rangle + \frac{\gamma_2}{2} \|w - \nabla_y u^{k+1}\|_2^2 \right\} \\ z^{k+1} &= \underset{z}{\operatorname{argmin}} \left\{ \lambda \langle 1, z - f \log z \rangle - \langle \lambda_3^k, z - \mathcal{A}u^{k+1} \rangle + \frac{\gamma_3}{2} \|z - \mathcal{A}u^{k+1}\|_2^2 \right\} \end{aligned} \quad (3.7)$$

Consider the u-subproblem

$$\begin{aligned} u^{k+1} &= \underset{u}{\operatorname{argmin}} \left\{ \frac{\mu}{2} \|\nabla u\|_2^2 + \langle \lambda_1^k, \nabla_x u - v^k \rangle + \langle \lambda_2^k, \nabla_y u - w^k \rangle + \langle \lambda_3^k, \mathcal{A}u - z^k \rangle \right. \\ & \quad \left. + \frac{\gamma_1}{2} \|\nabla_x u - v^k\|_2^2 + \frac{\gamma_2}{2} \|\nabla_y u - w^k\|_2^2 + \frac{\gamma_3}{2} \|\mathcal{A}u - z^k\|_2^2 \right\} \\ &= \underset{u}{\operatorname{argmin}} \left\{ \frac{\mu}{2} \|\nabla u\|_2^2 + \frac{\gamma_1}{2} \|\nabla_x u - v^k + \frac{\lambda_1^k}{\gamma_1}\|_2^2 + \frac{\gamma_2}{2} \|\nabla_y u - w^k + \frac{\lambda_2^k}{\gamma_2}\|_2^2 + \frac{\gamma_3}{2} \|\mathcal{A}u - z^k + \frac{\lambda_3^k}{\gamma_3}\|_2^2 \right\} \end{aligned}$$

Differentiating w.r.t u and equating to zero we get,

$$(\mu \nabla^T \nabla + \gamma_1 \nabla_x^T \nabla_x + \gamma_2 \nabla_y^T \nabla_y + \gamma_3 \mathcal{A}^* \mathcal{A}) u^{k+1} = \gamma_1 \nabla_x^T (v^k - \frac{\lambda_1^k}{\gamma_1}) + \gamma_2 \nabla_y^T (w^k - \frac{\lambda_2^k}{\gamma_2}) + \gamma_3 \mathcal{A}^* (z^k - \frac{\lambda_3^k}{\gamma_3}) \quad (3.8)$$

where \mathcal{A}^* is the conjugate transpose of the operator \mathcal{A} . Choosing $\gamma_1 = \gamma_2$, we can write the above expression as

$$(\gamma_3 \mathcal{A}^* \mathcal{A} - (\mu + \gamma_1) \Delta) u^{k+1} = \gamma_1 \nabla_x^T (v^k - \frac{\lambda_1^k}{\gamma_1}) + \gamma_2 \nabla_y^T (w^k - \frac{\lambda_2^k}{\gamma_2}) + \gamma_3 \mathcal{A}^* (z^k - \frac{\lambda_3^k}{\gamma_3}), \quad (3.9)$$

where $\Delta = -(\nabla_x^T \nabla_x + \nabla_y^T \nabla_y)$ denote the Laplace operator.

Consider the (v, w) -subproblem

$$\begin{aligned}
(v^{k+1}, w^{k+1}) &= \underset{v, w}{\operatorname{argmin}} \left\{ \|(v, w)\|_p^p - \langle \lambda_1^k, v - \nabla_x u^{k+1} \rangle + \frac{\gamma_1}{2} \|v - \nabla_x u^k\|_2^2 \right. \\
&\quad \left. - \langle \lambda_2^k, v - \nabla_y u^k \rangle + \frac{\gamma_2}{2} \|v - \nabla_y u^k\|_2^2 \right\} \\
&= \underset{v, w}{\operatorname{argmin}} \left\{ \|(v, w)\|_p^p + \frac{\gamma_1}{2} \|v - \nabla_x u^{k+1} - \frac{\lambda_1^k}{\gamma_1}\|_2^2 + \frac{\gamma_2}{2} \|w - \nabla_y u^{k+1} - \frac{\lambda_2^k}{\gamma_2}\|_2^2 \right\}
\end{aligned} \tag{3.10}$$

The p-shrinkage formula [16] can be used for solving the v, w sub-problems. Thus we get,

$$v^{k+1} = \max \left\{ r^k - \gamma_1^{p-2} (r^k)^{p-1}, 0 \right\} \frac{r_x^k}{r^k} := \operatorname{shrink}_p(r_x^k, \gamma_1) \tag{3.11}$$

$$w^{k+1} = \max \left\{ r^k - \gamma_2^{p-2} (r^k)^{p-1}, 0 \right\} \frac{r_y^k}{r^k} := \operatorname{shrink}_p(r_y^k, \gamma_2) \tag{3.12}$$

where $r_x^k = \nabla_x u^{k+1} + \frac{\lambda_1^k}{\gamma_1}$, $r_y^k = \nabla_y u^{k+1} + \frac{\lambda_2^k}{\gamma_2}$ and $r^k = \sqrt{(r_x^k)^2 + (r_y^k)^2}$.

Consider the z-subproblem

$$\begin{aligned}
z^{k+1} &= \underset{z}{\operatorname{argmin}} \left\{ \lambda \langle 1, z - f \log z \rangle - \langle \lambda_3^k, z - \mathcal{A}u^{k+1} \rangle + \frac{\gamma_3}{2} \|z - \mathcal{A}u^{k+1}\|_2^2 \right\} \\
&= \underset{z}{\operatorname{argmin}} \left\{ \lambda \langle 1, z - f \log z \rangle + \frac{\gamma_3}{2} \|z - \mathcal{A}u^{k+1} - \frac{\lambda_3^k}{\gamma_3}\|_2^2 \right\}
\end{aligned} \tag{3.13}$$

Differentiating R.H.S of (3.13) w.r.t z and equating with zero, we get the optimal condition for z as

$$z^2 - \left(\mathcal{A}u^{k+1} + \frac{\lambda_3}{\gamma_3} - \frac{\lambda}{\gamma_3} \right) z - \frac{\lambda}{\gamma_3} f = 0. \tag{3.14}$$

Thus we get

$$z^{k+1} = \frac{1}{2} \left(\left(\mathcal{A}u^{k+1} + \frac{\lambda_3}{\gamma_3} - \frac{\lambda}{\gamma_3} \right) + \sqrt{\left(\mathcal{A}u^{k+1} + \frac{\lambda_3}{\gamma_3} - \frac{\lambda}{\gamma_3} \right)^2 + \frac{4\lambda}{\gamma_3} f} \right). \tag{3.15}$$

4 Convergence Analysis

This section deals with the convergence of the sequence $\{u^k\}$ obtained by the algorithm proposed in the last section, to a minimizer $\{u^*\}$ of (3.4). For this, the following lemmas are needed.

Lemma 4.1. [10] *Let $E = E_1 + E_2$ Let $E_1, E_2 : \mathbb{R}^d \rightarrow \mathbb{R}$ be two l.s.c and convex functions and $E = E_1 + E_2$. Let E_1' be the Gateaux-derivative of the function E_1 then the following two statements are equivalent to each other:*

1. \exists a solution $x^* \in \mathbb{R}^d$ of the minimization problem $\inf_x E(x)$;
2. $E_2(x) - E_2(x^*) + \langle E_1'(x^*), x - x^* \rangle \geq 0, \forall x^* \in \mathbb{R}^d$.

Theorem 4.2. Let $\{u^k, v^k, w^k, z^k, \lambda_1^k, \lambda_2^k, \lambda_3^k\}$ be the sequence obtained by the proposed algorithm. Then

$$\begin{aligned} \lim_{k \rightarrow +\infty} \|v^{k+1} - v^k\|_2 &= 0, & \lim_{k \rightarrow +\infty} \|w^{k+1} - w^k\|_2 &= 0, & \lim_{k \rightarrow +\infty} \|z^{k+1} - z^k\|_2 &= 0 \\ \lim_{k \rightarrow +\infty} \|v^{k+1} - \nabla_x^k u^k\|_2 &= 0, & \lim_{k \rightarrow +\infty} \|w^{k+1} - \nabla_y^k u^k\|_2 &= 0, & \lim_{k \rightarrow +\infty} \|z^{k+1} - \mathcal{A}u^k\|_2 &= 0 \\ \lim_{k \rightarrow +\infty} \|\lambda_1^{k+1} - \lambda_1^k\|_2 &= 0, & \lim_{k \rightarrow +\infty} \|\lambda_2^{k+1} - \lambda_2^k\|_2 &= 0, & \lim_{k \rightarrow +\infty} \|\lambda_3^{k+1} - \lambda_3^k\|_2 &= 0 \end{aligned} \quad (4.1)$$

Proof. Assume $\{u^k, v^k, w^k, z^k, \lambda_1^k, \lambda_2^k, \lambda_3^k\}$ is the sequence obtained by the schemes (3.5)-(3.6). Let $(u^*, v^*, w^*, z^*, \lambda_1^*, \lambda_2^*, \lambda_3^*)$ be a saddle point of the function $\mathcal{L}(u, v, w, z, \lambda_1, \lambda_2, \lambda_3)$. Using the first part of the inequality (3.4), we get $v^* = \nabla_x u^*, w^* = \nabla_y u^*, z^* = \mathcal{A}u^*$. Using these relations and the equation (3.6) we have,

$$\begin{aligned} \lambda_1^* &= \lambda_1^* - \gamma_1 (v^* - \nabla_x u^*) \\ \lambda_2^* &= \lambda_2^* - \gamma_2 (w^* - \nabla_y u^*) \\ \lambda_3^* &= \lambda_3^* - \gamma_3 (z^* - \mathcal{A}u^*) \end{aligned} \quad (4.2)$$

Denote the error by $u_e^k = u^k - u^*, v_e^k = v^k - v^*, w_e^k = w^k - w^*, z_e^k = z^k - z^*, \lambda_{1(e)}^k = \lambda_1^k - \lambda_1^*, \lambda_{2(e)}^k = \lambda_2^k - \lambda_2^*, \lambda_{3(e)}^k = \lambda_3^k - \lambda_3^*$. Subtracting (4.2) from (3.6), we have

$$\begin{aligned} \lambda_{1(e)}^{k+1} &= \lambda_{1(e)}^k - \gamma_1 (v_e^{k+1} - \nabla_x u_e^{k+1}) \\ \lambda_{2(e)}^{k+1} &= \lambda_{2(e)}^k - \gamma_2 (w_e^{k+1} - \nabla_y u_e^{k+1}) \\ \lambda_{3(e)}^{k+1} &= \lambda_{3(e)}^k - \gamma_3 (z_e^{k+1} - \mathcal{A}u_e^{k+1}) \end{aligned} \quad (4.3)$$

Taking L^2 -norm on both sides, we have

$$\begin{aligned} \|\lambda_{1(e)}^{k+1}\|_2^2 &= \|\lambda_{1(e)}^k\|_2^2 + \gamma_1^2 \|v_e^{k+1} - \nabla_x u_e^{k+1}\|_2^2 - 2\gamma_1 \langle \lambda_{1(e)}^k, v_e^{k+1} - \nabla_x u_e^{k+1} \rangle \\ \|\lambda_{2(e)}^{k+1}\|_2^2 &= \|\lambda_{2(e)}^k\|_2^2 + \gamma_2^2 \|w_e^{k+1} - \nabla_y u_e^{k+1}\|_2^2 - 2\gamma_2 \langle \lambda_{2(e)}^k, w_e^{k+1} - \nabla_y u_e^{k+1} \rangle \\ \|\lambda_{3(e)}^{k+1}\|_2^2 &= \|\lambda_{3(e)}^k\|_2^2 + \gamma_3^2 \|z_e^{k+1} - \mathcal{A}u_e^{k+1}\|_2^2 - 2\gamma_3 \langle \lambda_{3(e)}^k, z_e^{k+1} - \mathcal{A}u_e^{k+1} \rangle \end{aligned} \quad (4.4)$$

From equation (3.3) and Lemma (4.1), we have

$$\begin{aligned} \langle \nabla_x^T \lambda_1^* + \nabla_y^T \lambda_2^* + \mathcal{A}^* \lambda_3^*, u - u^* \rangle + \mu \langle \nabla^T \nabla u^*, u - u^* \rangle + \gamma_1 \langle \nabla_x^T (\nabla_x u^* - v^*), u - u^* \rangle \\ + \gamma_2 \langle \nabla_y^T (\nabla_y u^* - w^*), u - u^* \rangle + \gamma_3 \langle \mathcal{A}^* (\mathcal{A}u^* - z^*), u - u^* \rangle \geq 0 \end{aligned} \quad (4.5)$$

and

$$(\|(v, w)\|_p^p - \|(v^*, w)\|_p^p) - \langle \lambda_1^*, v - v^* \rangle + \gamma_1 \langle v^* - \nabla_x u^*, v - v^* \rangle \geq 0 \quad (4.6)$$

and

$$(\|(v, w)\|_p^p - \|(v, w^*)\|_p^p) - \langle \lambda_2^*, w - w^* \rangle + \gamma_2 \langle w^* - \nabla_y u^*, w - w^* \rangle \geq 0 \quad (4.7)$$

and

$$\lambda (\langle 1, z - f \log z \rangle - \langle 1, z^* - f \log z^* \rangle) - \langle \lambda_3^*, z - z^* \rangle + \gamma_3 \langle z^* - \mathcal{A}u^*, z - z^* \rangle \geq 0 \quad (4.8)$$

For $u^k, v^k, w^k, z^k, \lambda_1^k, \lambda_2^k$ and λ_3^k , u^{k+1} is solution of u -sub-problem. Using Lemma(4.1) gives, we have

$$\begin{aligned} & \left\langle \nabla_x^T \lambda_1^k + \nabla_y^T \lambda_2^k + \mathcal{A}^* \lambda_3^k, u - u^{k+1} \right\rangle + \mu \left\langle \nabla^T \nabla u^{k+1}, u - u^{k+1} \right\rangle + \gamma_1 \left\langle \nabla_x^T (\nabla_x u^{k+1} - v^k), u - u^{k+1} \right\rangle \\ & + \gamma_2 \left\langle \nabla_y^T (\nabla_y u^{k+1} - w^k), u - u^{k+1} \right\rangle + \gamma_3 \left\langle \mathcal{A}^* (\mathcal{A} u^{k+1} - z^k), u - u^{k+1} \right\rangle \geq 0 \end{aligned} \quad (4.9)$$

Substituting $u = u^*$ in (4.9) and $u = u^{k+1}$ in (4.5) respectively and then adding them, we get

$$\begin{aligned} & \left\langle \lambda_{1(e)}^k, \nabla_x u_e^{k+1} \right\rangle + \left\langle \lambda_{2(e)}^k, \nabla_y u_e^{k+1} \right\rangle + \left\langle \lambda_{3(e)}^k, \mathcal{A} u_e^{k+1} \right\rangle - \mu \left\langle \nabla u_e^{k+1}, \nabla u_e^{k+1} \right\rangle + \\ & \gamma_1 \left\langle \nabla_x u_e^{k+1} - v_e^k, \nabla_x u_e^{k+1} \right\rangle + \gamma_2 \left\langle \nabla_y u_e^{k+1} - w_e^k, \nabla_y u_e^{k+1} \right\rangle + \gamma_3 \left\langle \mathcal{A} u_e^{k+1} - z_e^k, \mathcal{A} u_e^{k+1} \right\rangle \leq 0 \end{aligned} \quad (4.10)$$

In a similarly way, we have

$$\left\langle \lambda_{1(e)}^k, -v_e^{k+1} \right\rangle + \gamma_1 \left\langle v_e^{k+1} - \nabla_x u_e^{k+1}, v_e^{k+1} \right\rangle \leq 0 \quad (4.11)$$

$$\left\langle \lambda_{2(e)}^k, -w_e^{k+1} \right\rangle + \gamma_2 \left\langle w_e^{k+1} - \nabla_y u_e^{k+1}, w_e^{k+1} \right\rangle \leq 0 \quad (4.12)$$

$$\left\langle \lambda_{3(e)}^k, -z_e^{k+1} \right\rangle + \gamma_3 \left\langle z_e^{k+1} - \mathcal{A} u_e^{k+1}, z_e^{k+1} \right\rangle \leq 0 \quad (4.13)$$

Adding all the equations from (4.10) to equation (4.13) up, we have

$$\begin{aligned} & \left\langle \lambda_{1(e)}^k, v_e^{k+1} - \nabla_x u_e^{k+1} \right\rangle + \left\langle \lambda_{2(e)}^k, w_e^{k+1} - \nabla_y u_e^{k+1} \right\rangle + \left\langle \lambda_{3(e)}^k, z_e^{k+1} - \mathcal{A} u_e^{k+1} \right\rangle \geq \mu \|\nabla u_e^{k+1}\|_2^2 \\ & + \gamma_1 \left\langle v_e^{k+1} - v_e^k, \nabla_x u_e^{k+1} \right\rangle + \gamma_2 \left\langle w_e^{k+1} - w_e^k, \nabla_y u_e^{k+1} \right\rangle + \gamma_3 \left\langle z_e^{k+1} - z_e^k, \mathcal{A} u_e^{k+1} \right\rangle \\ & + \gamma_1 \|v_e^{k+1} - \nabla_x u_e^{k+1}\|_2^2 + \gamma_2 \|w_e^{k+1} - \nabla_y u_e^{k+1}\|_2^2 + \gamma_3 \|z_e^{k+1} - \mathcal{A} u_e^{k+1}\|_2^2 \end{aligned} \quad (4.14)$$

Using (4.4) into (4.14), we have

$$\begin{aligned} & \frac{1}{\gamma_1} \left(\|\lambda_{1(e)}^k\|_2^2 - \|\lambda_{1(e)}^{k+1}\|_2^2 \right) + \frac{1}{\gamma_2} \left(\|\lambda_{2(e)}^k\|_2^2 - \|\lambda_{2(e)}^{k+1}\|_2^2 \right) + \frac{1}{\gamma_3} \left(\|\lambda_{3(e)}^k\|_2^2 - \|\lambda_{3(e)}^{k+1}\|_2^2 \right) \geq 2\mu \|\nabla u_e^{k+1}\|_2^2 \\ & + 2\gamma_1 \left\langle v_e^{k+1} - v_e^k, \nabla_x u_e^{k+1} \right\rangle + 2\gamma_2 \left\langle w_e^{k+1} - w_e^k, \nabla_y u_e^{k+1} \right\rangle + 2\gamma_3 \left\langle z_e^{k+1} - z_e^k, \mathcal{A} u_e^{k+1} \right\rangle \\ & + \gamma_1 \|v_e^{k+1} - \nabla_x u_e^{k+1}\|_2^2 + \gamma_2 \|w_e^{k+1} - \nabla_y u_e^{k+1}\|_2^2 + \gamma_3 \|z_e^{k+1} - \mathcal{A} u_e^{k+1}\|_2^2 \end{aligned} \quad (4.15)$$

Form (4.6), we have

$$\left(\|(v, w)\|_p^p - \|(v^{k+1}, w)\|_p^p \right) - \left\langle \lambda_1^k, v - v^{k+1} \right\rangle + \gamma_1 \left\langle v^{k+1} - \nabla_x u^{k+1}, v - v^{k+1} \right\rangle \geq 0 \quad (4.16)$$

that is

$$\left(\|(v, w)\|_p^p - \|(v^k, w)\|_p^p \right) - \left\langle \lambda_1^{k-1}, v - v^k \right\rangle + \gamma_1 \left\langle v^k - \nabla_x u^k, v - v^k \right\rangle \geq 0 \quad (4.17)$$

Putting $v = v^k$ in (4.16) and $v = v^{k+1}$ in (4.17) and adding the resultant, we have

$$\gamma_1 \|v_e^{k+1} - v_e^k\|_2^2 - \left\langle \lambda_{1(e)}^k - \lambda_{1(e)}^{k-1}, v_e^{k+1} - v_e^k \right\rangle - \gamma_1 \left\langle (\nabla_x u_e^{k+1} - v_e^{k+1}) - (\nabla_x u_e^k - v_e^k), v_e^{k+1} - v_e^k \right\rangle \leq 0 \quad (4.18)$$

Using the first equation of (4.3) with $k = k - 1$ in (4.18), we have

$$\left\langle v_e^{k+1} - v_e^k, \nabla_x u_e^{k+1} - v_e^k \right\rangle \geq \|v_e^{k+1} - v_e^k\|_2^2 \quad (4.19)$$

Since $\langle v_e^{k+1} - v_e^k, v_e^k \rangle = \frac{1}{2} (\|v_e^{k+1}\|_2^2 - \|v_e^k\|_2^2 - \|v_e^{k+1} - v_e^k\|_2^2)$. So, the equation (4.19) implies

$$2 \left\langle v_e^{k+1} - v_e^k, \nabla_x u_e^{k+1} \right\rangle \geq \left(\|v_e^{k+1}\|_2^2 - \|v_e^k\|_2^2 - \|v_e^{k+1} - v_e^k\|_2^2 \right) \quad (4.20)$$

Arguing in a similar manner, we get

$$2 \left\langle w_e^{k+1} - w_e^k, \nabla_y u_e^{k+1} \right\rangle \geq \left(\|w_e^{k+1}\|_2^2 - \|w_e^k\|_2^2 - \|w_e^{k+1} - w_e^k\|_2^2 \right) \quad (4.21)$$

and

$$2 \left\langle z_e^{k+1} - z_e^k, \mathcal{A}u_e^{k+1} \right\rangle \geq \left(\|z_e^{k+1}\|_2^2 - \|z_e^k\|_2^2 - \|z_e^{k+1} - z_e^k\|_2^2 \right) \quad (4.22)$$

Substituting (4.20) – (4.22) into (4.15), we get

$$\begin{aligned} & \frac{1}{\gamma_1} \left(\|\lambda_{1(e)}^k\|_2^2 - \|\lambda_{1(e)}^{k+1}\|_2^2 \right) + \frac{1}{\gamma_2} \left(\|\lambda_{2(e)}^k\|_2^2 - \|\lambda_{2(e)}^{k+1}\|_2^2 \right) + \frac{1}{\gamma_3} \left(\|\lambda_{3(e)}^k\|_2^2 - \|\lambda_{3(e)}^{k+1}\|_2^2 \right) \\ & + \gamma_1 \left(\|v_e^k\|_2^2 - \|v_e^{k+1}\|_2^2 \right) + \gamma_2 \left(\|w_e^k\|_2^2 - \|w_e^{k+1}\|_2^2 \right) + \gamma_3 \left(\|z_e^k\|_2^2 - \|z_e^{k+1}\|_2^2 \right) \geq \\ & \gamma_1 \left(\|v_e^{k+1} - v_e^k\|_2^2 \right) + \gamma_2 \left(\|w_e^{k+1} - w_e^k\|_2^2 \right) + \gamma_3 \left(\|z_e^{k+1} - z_e^k\|_2^2 \right) + 2\mu \|\nabla u_e^{k+1}\|_2^2 \\ & + \gamma_1 \|v_e^{k+1} - \nabla_x u_e^{k+1}\|_2^2 + \gamma_2 \|w_e^{k+1} - \nabla_y u_e^{k+1}\|_2^2 + \gamma_3 \|z_e^{k+1} - \mathcal{A}u_e^{k+1}\|_2^2 \end{aligned} \quad (4.23)$$

Putting $k = 0, 1, \dots, N$ and adding the results, we get

$$\begin{aligned} & \frac{1}{\gamma_1} \left(\|\lambda_{1(e)}^0\|_2^2 - \|\lambda_{1(e)}^{N+1}\|_2^2 \right) + \frac{1}{\gamma_2} \left(\|\lambda_{2(e)}^0\|_2^2 - \|\lambda_{2(e)}^{N+1}\|_2^2 \right) + \frac{1}{\gamma_3} \left(\|\lambda_{3(e)}^0\|_2^2 - \|\lambda_{3(e)}^{N+1}\|_2^2 \right) \\ & + \gamma_1 \left(\|v_e^0\|_2^2 - \|v_e^{N+1}\|_2^2 \right) + \gamma_2 \left(\|w_e^0\|_2^2 - \|w_e^{N+1}\|_2^2 \right) + \gamma_3 \left(\|z_e^0\|_2^2 - \|z_e^{N+1}\|_2^2 \right) \\ & \geq \gamma_1 \sum_{k=0}^N \left(\|v_e^{k+1} - v_e^k\|_2^2 \right) + \gamma_2 \sum_{k=0}^N \left(\|w_e^{k+1} - w_e^k\|_2^2 \right) + \gamma_3 \sum_{k=0}^N \left(\|z_e^{k+1} - z_e^k\|_2^2 \right) \\ & + \gamma_1 \sum_{k=0}^N \|v_e^{k+1} - \nabla_x u_e^{k+1}\|_2^2 + \gamma_2 \sum_{k=0}^N \|w_e^{k+1} - \nabla_y u_e^{k+1}\|_2^2 + \gamma_3 \sum_{k=0}^N \|z_e^{k+1} - \mathcal{A}u_e^{k+1}\|_2^2 \end{aligned} \quad (4.24)$$

which implies that $\{u^k\}, \{v^k\}, \{w^k\}, \{z^k\}, \{\lambda_1^k\}, \{\lambda_2^k\}, \{\lambda_3^k\}, \{\nabla_x u^k\}, \{\nabla_y u^k\}$ and $\{\mathcal{A}u^k\}$ are bounded. Hence the required result (4.1) follows from (4.24) and (4.3).

Theorem 4.3. The sequence $\{u^k\}$ obtained by the formula (??) approaches to the minimizer u^* of the proposed model (3.1), provided \mathcal{A} is injective.

Proof. As $(u^*, v^*, w^*, z^*, \lambda_1^*, \lambda_2^*, \lambda_3^*)$ is a saddle point of $\mathcal{L}(u, v, w, z, \lambda_1, \lambda_2, \lambda_3)$, the last inequality of (3.4) and (4.1), we get

$$\begin{aligned} \frac{\mu}{2} \|\nabla u^*\|_2^2 + \|(v^*, w^*)\|_p^p + \lambda \langle 1, z^* - f \log z^* \rangle \leq \lim_{k \rightarrow \infty} \left(\frac{\mu}{2} \|\nabla u^{k+1}\| + \|(v^{k+1}, w^{k+1})\|_p^p \right. \\ \left. + \lambda \langle 1, z^{k+1} - f \log z^{k+1} \rangle \right) \end{aligned} \quad (4.25)$$

Putting v^*, w^*, z^* in the $(v, w), z$ -subproblems, respectively and substituting $u = u^*$ in (4.9) and then adding the corresponding results, we have

$$\begin{aligned} \frac{\mu}{2} \|\nabla u^*\|_2^2 + \|(v^*, w^*)\|_p^p + \lambda \langle 1, z^* - f \log z^* \rangle \geq \frac{\mu}{2} \|\nabla u^{k+1}\| + \|(v^{k+1}, w^{k+1})\|_p^p \\ + \lambda \langle 1, z^{k+1} - f \log z^{k+1} \rangle \end{aligned} \quad (4.26)$$

On taking limit in (4.26) and then combining the resultant with Lemma(4.1) we have

$$\begin{aligned} \frac{\mu}{2} \|\nabla^*\|_2^2 + \|(v^*, w^*)\|_p^p + \lambda \langle 1, z^* - f \log z^* \rangle \geq \lim_{k \rightarrow \infty} \left(\frac{\mu}{2} \|\nabla u^{k+1}\| + \|(v^{k+1}, w^{k+1})\|_p^p \right. \\ \left. + \lambda \langle 1, z^{k+1} - f \log z^{k+1} \rangle \right) \end{aligned} \quad (4.27)$$

By (4.25) and (4.27), we have

$$\begin{aligned} \frac{\mu}{2} \|\nabla^*\|_2^2 + \|(v^*, w^*)\|_p^p + \lambda \langle 1, z^* - f \log z^* \rangle = \lim_{k \rightarrow \infty} \left(\frac{\mu}{2} \|\nabla u^{k+1}\| + \|(v^{k+1}, w^{k+1})\|_p^p \right. \\ \left. + \lambda \langle 1, z^{k+1} - f \log z^{k+1} \rangle \right) \end{aligned} \quad (4.28)$$

This together with $v = \nabla_x u, w = \nabla_y u, z = \mathcal{A}u$ gives that

$$\begin{aligned} \frac{\mu}{2} \|\nabla^*\|_2^2 + \|(v^*, w^*)\|_p^p + \lambda \langle 1, z^* - f \log z^* \rangle = \\ \lim_{k \rightarrow \infty} \left(\frac{\mu}{2} \|\nabla u^{k+1}\| + \|(\nabla_x u^{k+1}, \nabla_y u^{k+1})\|_p^p + \lambda \langle 1, \mathcal{A}u^{k+1} - f \log \mathcal{A}u^{k+1} \rangle \right) \end{aligned} \quad (4.29)$$

The continuity of the functions (3.1),(4.1) and the result (4.29) implies $\{u^k\}$ is minimizing sequence. Using the injective property of \mathcal{A} we get $\lim_{k \rightarrow \infty} \|u^k - u^*\|_2^2 = 0$.

5 Numerical Results

We present the numerical results of our model on some standard test images and compare them with the that of the models proposed in [7]and [15]. Note that if we put $\mu = 0, p = 1$ then our model reduces to TV model proposed in [6, 7] and if $\mu \neq 0, p = 1$ then it reduces to the model proposed in [15]. We have used used Augmented Lagrangian method for our model and the model [15] whereas Split Bregman method has been used for TV model [6]. So, we call the TV-model as TVSB model. For implementing the code and the selection of the parameters we have followed the paper [14] and the code shared by the author. We use the stop the iteration process while the relative error between two consecutive iterates is less than given tolerance value ϵ_{tol} that is

$$\frac{\|u^{k+1} - u^k\|_2}{\|u^k\|_2} \leq \epsilon_{tol}, \quad (5.1)$$

or it reaches the maximum iterations which we set as 250. Here we choose $\epsilon_{tol} = 10^{-4}$. The parameters our models are as follows: $\mu = 0.01, \gamma_1 = 0.5 = \gamma_2, \gamma_3 = 30$. The fidelity parameter λ is selected by trail and error method which we mentioned later. The choice of the parameters are influenced by the existing models in the literature. Although, the value of p can be any value in the interval $(0, 1]$, the best result is obtained while we choose $p = \frac{1}{2}$ [16]. So we have used $p = \frac{1}{2}$ in the experiments.

To compare the results, the image quality metric Peak-signal to noise ratio (PSNR), Signal to noise ratio (SNR) and SSIM [20] have been calculated. Let u be resulting image and I is the true image of dimension $m \times n$. Then these quantities are defined by:

$$PSNR = 10 \log_{10} \frac{255^2}{(1/mn) \sum_{i=1}^m \sum_{j=1}^n (u_{i,j} - I_{i,j})^2},$$

$$SNR = 20 \log_{10} \left(\frac{\|I\|_2}{\|I - u\|_2} \right),$$

and

$$SSIM = \frac{(2\mu_u\mu_I + C_1)(2\sigma_{uI} + C_2)}{(\mu_u^2 + \mu_I^2 + C_1)(\sigma_u^2 + \sigma_I^2 + C_2)}$$

where μ_v represents the mean of $v = u/I$ and σ_v represents the variance of $v = u/I$ and σ_{IU} represent the covariance between I and u , C_i are constants for $i = 1, 2$. SSIM indicates how the image u is structurally similar to the true image I . Higher the values of these quantities, better the recovered image.

5.1 Removing Poisson Noise

In this subsection, we present denoising result of three images corrupted with Poisson noise only. We use the MATLAB command 'imnoise' to add the Poisson noise in the image.

In Figure 1, we have reported the denoising results of a synthetic image of size 128×128 , corrupted with Poisson noise, using our model, $\ell_2 - \ell_1$ model and TV model. We set the fidelity parameter as $\lambda = 6$ for this image. In order to compare our result, we have reported the metric SSIM, PSNR and SNR corresponding to the result of three models in Table 1. From the Table one can see that the PSNR, SNR are higher for our model that implies that the performance of our proposed model is better than the other two. Also, we have reported the CPU time in the table. The TV model consuming less time than the other two.

In Figure 2, we have reported the denoising results of the Lena image of dimension 256×256 , corrupted with Poisson noise, using our model, $\ell_2 - \ell_1$ model and TV model. For this image, we choose the fidelity parameter $\lambda = 7$. The image quality metric SSIM, PSNR, and SNR are reported in Table 1. Looking at the values reported in Table 1, one can note that the SSIM, PSNR and SNR corresponding to the result of our model higher than that of the other two models which implies that our result is much better than the other two models. The highest CPU time is taken by $\ell_2 - \ell_1$ model.

In Figure 3, we have presented the denoising results of the peppers image of dimension 256×256 , corrupted by Poisson noise, using our model, $\ell_2 - \ell_1$ model and TV model. The fidelity parameter is chosen as $\lambda = 5$. The PSNR, SNR are same for our model and $\ell_2 - \ell_1$ model but SSIM is higher than that of $\ell_2 - \ell_1$ model. All the three metrics is higher than the TV Model. So our model gives better result than the other two models at-least in SSIM.

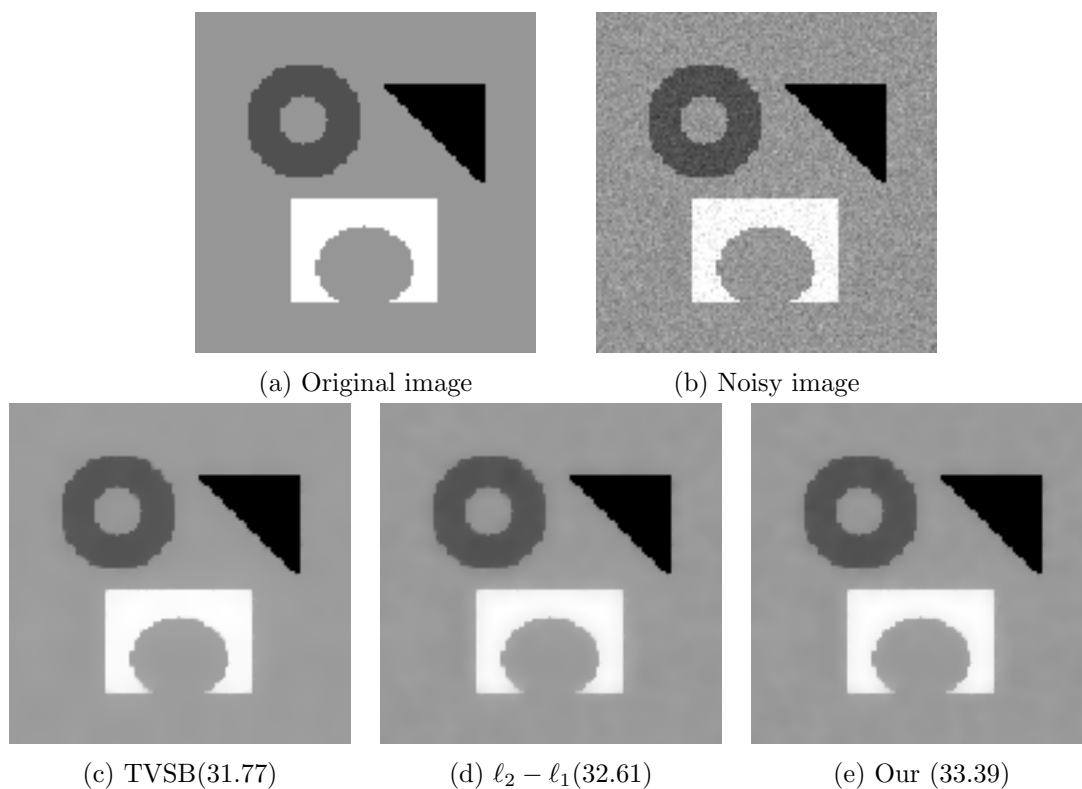


Figure 1: Comparison of denoising results of a synthetic image corrupted with Poisson noise. PSNR values are indicated in bracket.

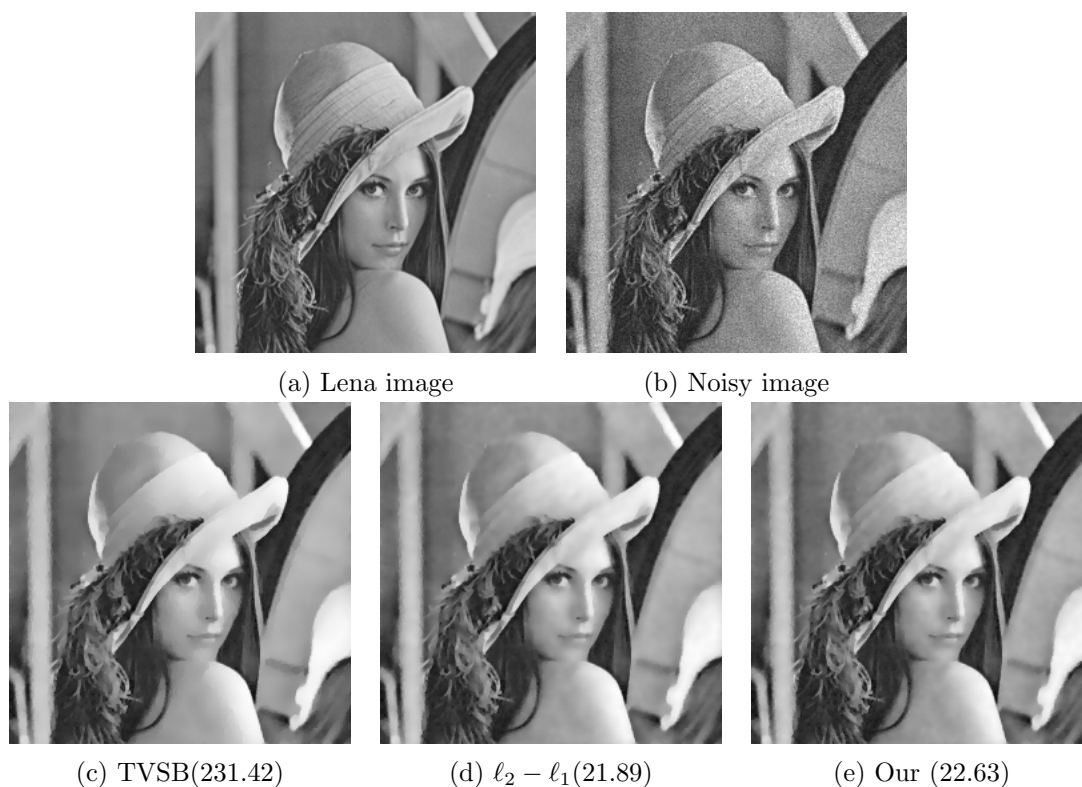


Figure 2: Comparison of denoising results of Lena image corrupted with Poisson noise. PSNR values are indicated in bracket.

Image	Model	PSNR	SNR	SSIM	Iterations	CPU
Synthetic	$TV - SB$	31.77	27.37	0.9887	42	0.11
	$\ell_2 - \ell_1$	32.61	28.22	0.9771	67	0.17
	Our ($p = 1/2$)	33.39	28.99	0.9793	60	0.15
Lena	$TV - SB$	21.42	15.58	0.8773	39	0.46
	$\ell_2 - \ell_1$	21.89	16.05	0.8779	60	0.67
	Our ($p = 1/2$)	22.63	16.79	0.8861	50	0.57
Peppers	$TV - SB$	19.40	13.85	0.8579	43	0.50
	$\ell_2 - \ell_1$	20.21	14.66	0.8629	63	0.70
	Our ($p = 1/2$)	20.22	14.67	0.8722	56	0.63

Table 1: Comparison of results of images degraded by Poisson noise.

5.2 Removing Poisson noise with motion blur

In this subsection, we present the denoising result of images corrupted with Poisson noise in presence of motion blur. First the motion filter is created using the MATLAB command 'fspecial' and applied to the image using command 'imfilter' to create blurry image. Then, we add Poisson noise to the blurry image. In order to compare our results, we have reported the SSIM, PSNR and SNR in Table 2.

In Figure 4, we have reported the denoising results of a synthetic image of dimension 128×128 using our model, $\ell_2 - \ell_1$ model and TV model. The image is degraded by motion blur of radius 10 and $\theta = 90$ and Poisson noise. We chose the parameter $\lambda = 8$. From the Table2, one can see that the PSNR for the result of our model is 28.03 and that of TV model is 27.14, which indicates that our result is better for this image. SSIM, PSNR and SNR corresponding to our result is higher than that of other two models that clearly indicates that our model is better.

In Figure 5, we have reported the denoising results of the Lena image of dimension 256×256 using our model, $\ell_2 - \ell_1$ model and TV model. The image is degraded by motion blur of radius 10 and $\theta = 90$ and Poisson noise. We chose the fidelity parameters $\lambda = 8$ for this image. In this case, our model gives better result than TV model but the result of $\ell_2 - \ell_1$ model is also good. The CPU time taken by TV model is less that that of other two models.

In Figure 6, we have considered the peppers image of dimension 256×256 and degraded by the motion blur of radius 10 and $\theta = 90$ and added the Poisson noise. The original image and the noisy image are reported in the first row of Figure 6. The denoising results of the noisy peppers image using our model, $\ell_2 - \ell_1$ model and TV model are reported in the second row. We chose the fidelity parameters $\lambda = 10$ for this image. For this image, our model performs better than TV model $\ell_2 - \ell_1$ model in terms of SSIM, SNR and PSNR.

5.3 Removing Poisson noise with Gaussian blur

In this subsection, we present the denoising result of images corrupted by Poisson noise and having Gaussian blur. First the Gaussian blur is created using the MATLAB command 'fspecial' and applied to the image using command 'imfilter'. Then we add Poisson noise using the MATLAB command 'imnoise'. To compare the results, we calculated the image quality metric SNR, PSNR and SSIM for the result of this subsection of all three models are reported in Table 3.

In Figure 7, we have reported the denoising results of the synthetic image using our model, $\ell_2 - \ell_1$ model and TV model. The image is degraded by Gaussian blur of radius 3 and standard deviation $\sigma = 3$ and Poisson noise. We chose the parameter $\lambda = 8$. From the figure, one can

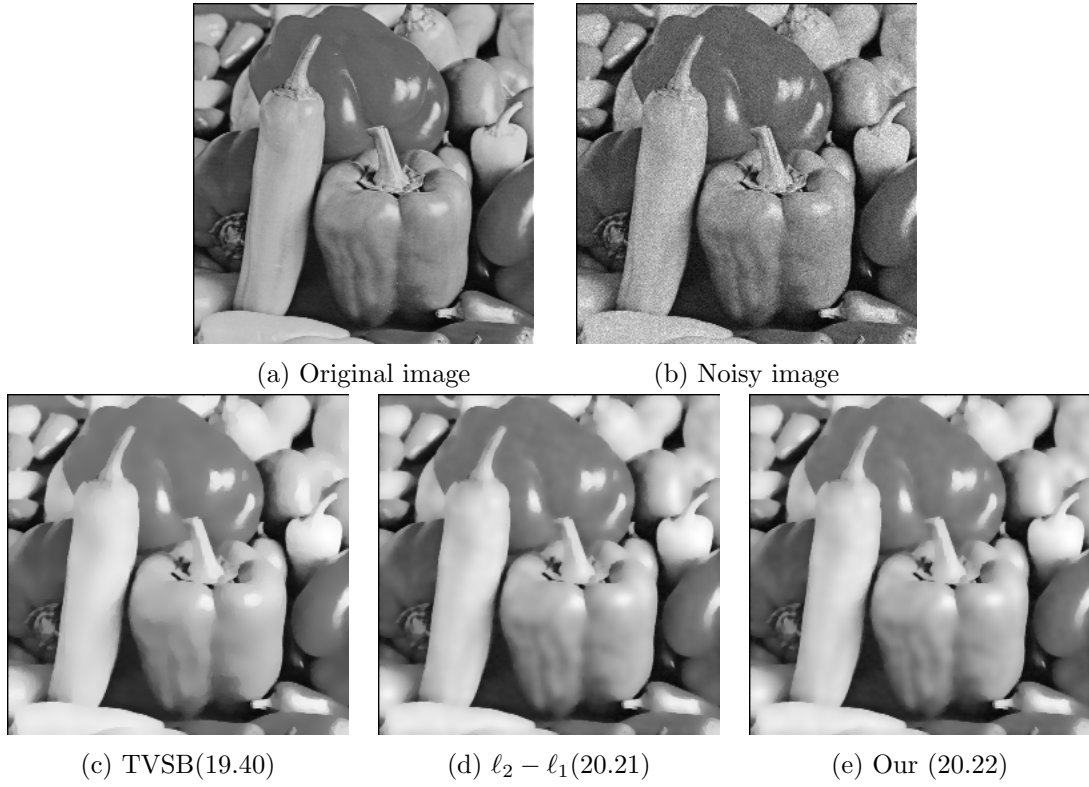


Figure 3: Comparison of denoising results of Peppers image corrupted with Poisson noise. PSNR values are indicated in bracket.

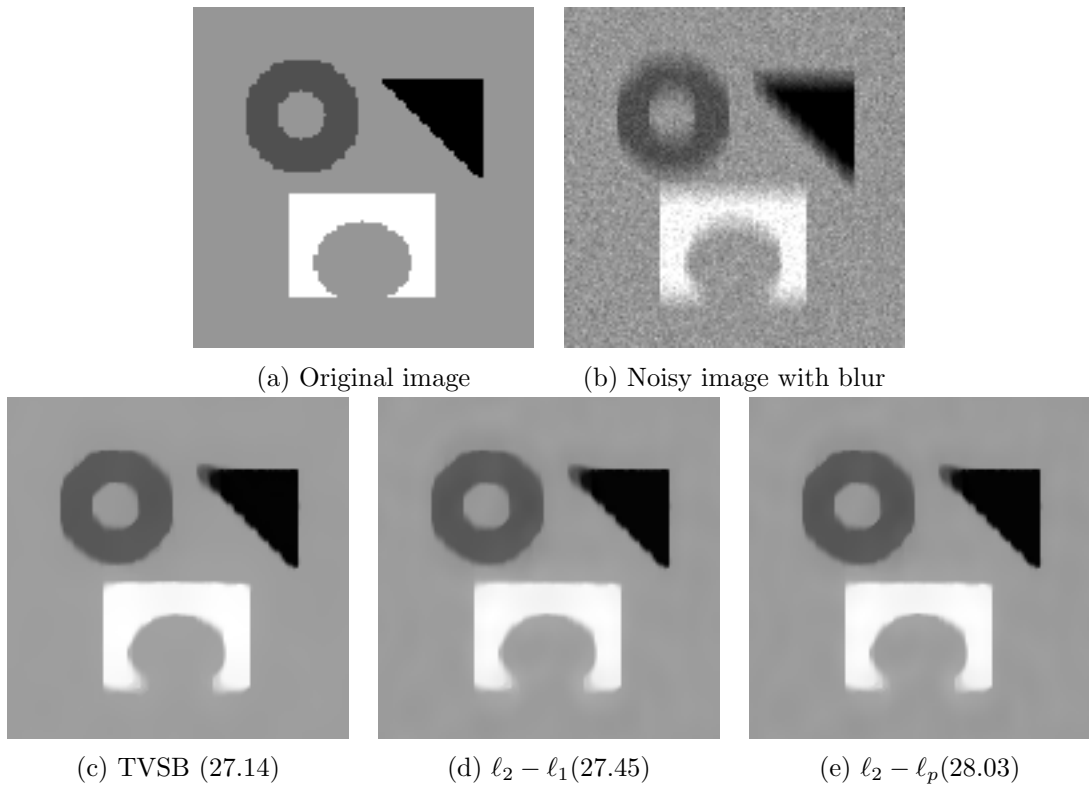


Figure 4: Comparison of denoising results of a synthetic image corrupted with Poisson noise having motion blur of size 10 and $\theta = 90$. PSNR values are indicated in bracket.

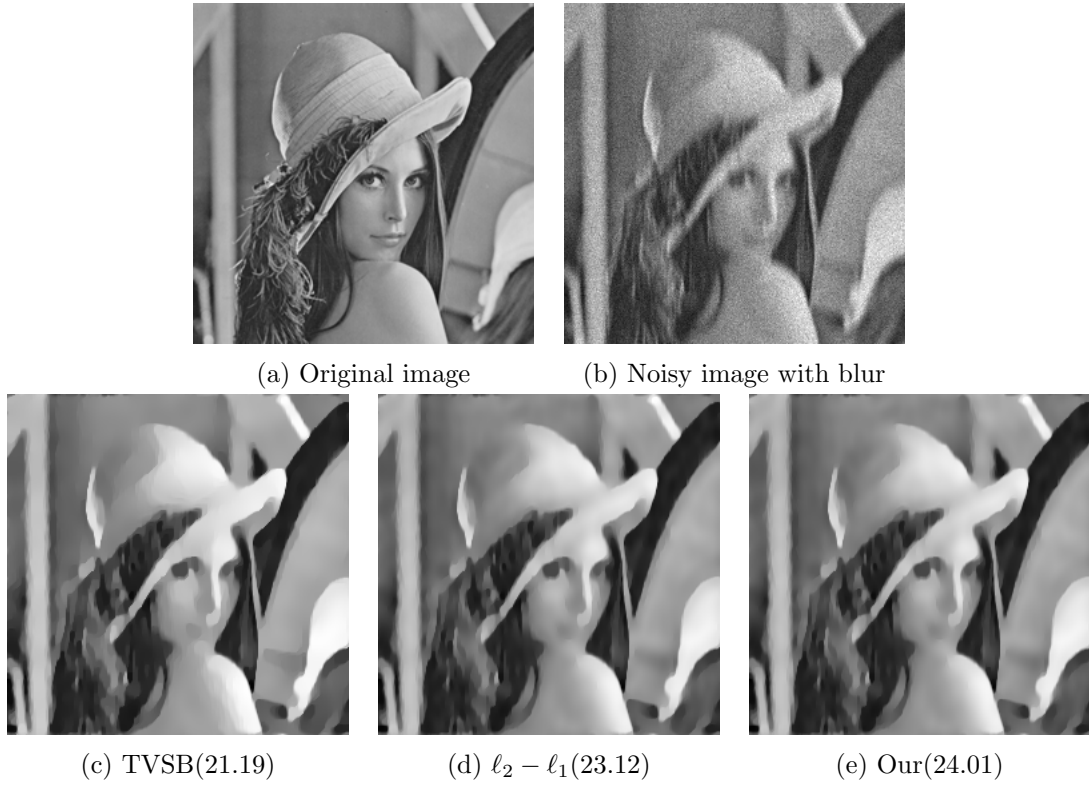


Figure 5: Denoising results of our model of the Lena image with motion blur and Poisson noise. PSNR values are indicated in bracket.

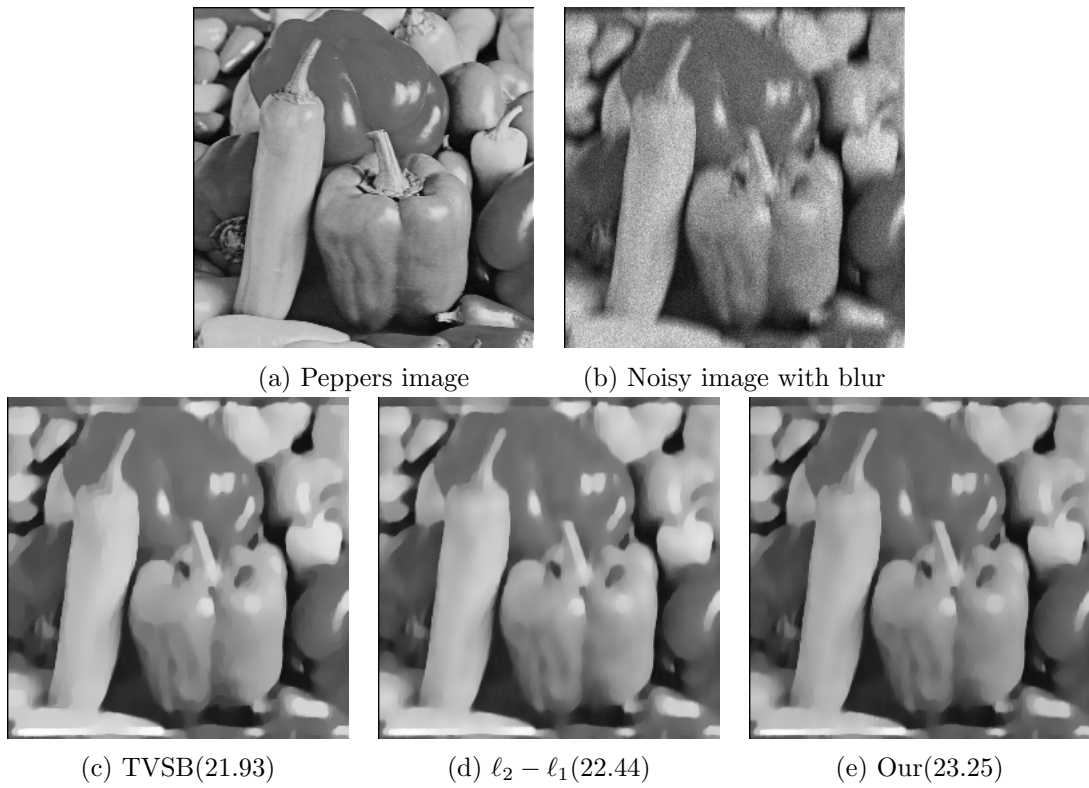


Figure 6: Denoising results of our model of the peppers image with motion blur and Poisson noise. PSNR values are indicated in bracket.

Image	Model	PSNR	SNR	SSIM	Iterations	CPU
Synthetic	$TV - SB$	27.14	22.75	0.9393	68	0.20
	$\ell_2 - \ell_1$	27.45	23.05	0.9250	96	0.29
	Our ($p = 1/2$)	28.03	23.63	0.9327	88	0.27
Lena	$TV - SB$	21.19	15.35	0.7732	70	0.81
	$\ell_2 - \ell_1$	23.12	17.28	0.7754	102	1.12
	Our ($p = 1/2$)	24.01	18.17	0.7806	93	1.01
Peppers	$TV - SB$	21.93	16.38	0.7529	69	0.76
	$\ell_2 - \ell_1$	22.44	16.89	0.7565	101	1.12
	Our ($p = 1/2$)	23.25	17.70	0.7604	110	1.20

Table 2: Comparison of denoising results obtained TV model and our model on motion blurred Images with Poisson noise.

see that the edges are sharp for our model. Looking at the values reported in Table 3, it can be said that the performance of our proposed model is better.

In Figure 8, we have reported the denoising result of the Lena image, degraded by Gaussian blur of radius 3 and standard deviation $\sigma = 3$ and Poisson noise, using our model, $\ell_2 - \ell_1$ model and TV model. We chose the parameters $\lambda = 6$. From the Table 3, one can see that the SSIM, PSNR and SNR for the result of our model is higher than that of $\ell_2 - \ell_1$ and TV model that implies our result is better.

In Figure 9, we have reported the denoising result of the Peppers image using our model, $\ell_2 - \ell_1$ model and TV model. The image is degraded by Gaussian blur of radius 3 and standard deviation $\sigma = 3$ and Poisson noise. We chose the parameters $\lambda = 6, \gamma_3 = 25$. From the Figure 9 one can notice that our model performs better. The SSIM, PSNR and SNR for the result of our model is higher than that of $\ell_2 - \ell_1$ and TV models that implies our result is better.

Image	Model	PSNR	SNR	SSIM	Iterations	CPU
Synthetic	$TV - SB$	28.91	24.52	0.9499	41	0.12
	$\ell_2 - \ell_1$	29.45	25.05	0.9355	69	0.26
	Our ($p = 1/2$)	29.92	25.43	0.9387	62	0.23
Lena	$TV - SB$	22.01	16.17	0.8089	55	0.74
	$\ell_2 - \ell_1$	23.39	17.55	0.8080	96	1.25
	Our($p = 1/2$)	26.69	20.85	0.8162	86	1.11
Peppers	$TV - SB$	20.15	14.60	0.7949	56	0.61
	$\ell_2 - \ell_1$	21.92	16.37	0.8009	82	0.91
	Our($p = 1/2$)	24.97	19.42	0.8052	79	0.89

Table 3: Comparison of results of images degraded by Gaussian blur and Poisson noise.

6 Conclusion

A variational PDE based model has been proposed. We have used augmented Lagrangian method to solve our model. The convergence analysis have been carried out for our numerical scheme. The numerical results of our model are compared with the results of $\ell_2 - \ell_1$ model and TV model. To quantify the results the image quality metric SSIM, PSNR and SNR has been calculated. All three quantities are higher for our result, which implies that our model is better than the TV and $\ell_2 - \ell_1$ model.

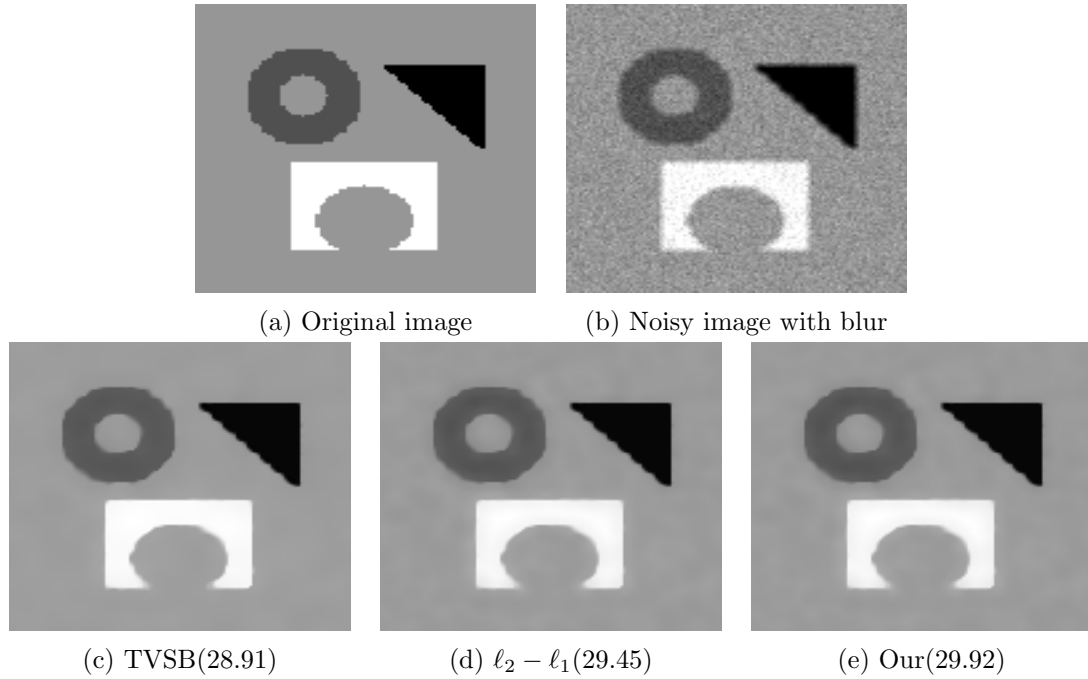


Figure 7: Comparison of denoising results of our model on a synthetic image with Gaussian blur with and Poisson noise. PSNR values are reported in bracket.

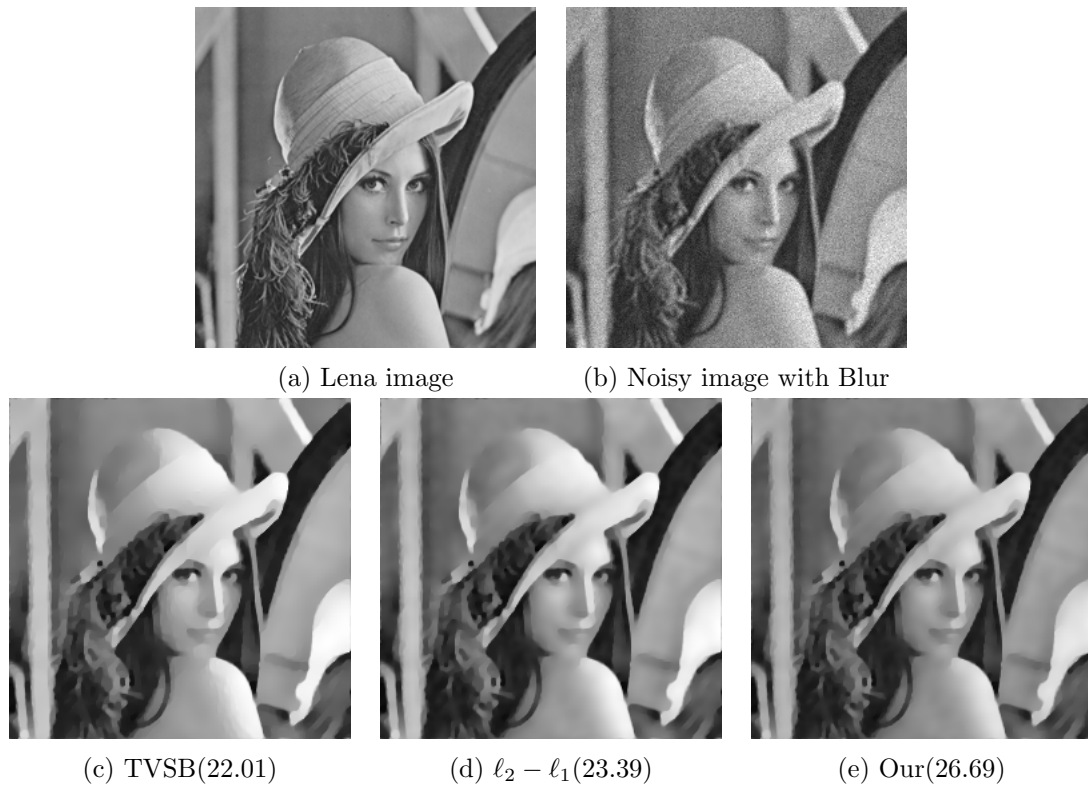


Figure 8: Comparison of denoising results of our model on Lena image with Gaussian blur and Poisson noise. PSNR values are indicated in bracket.

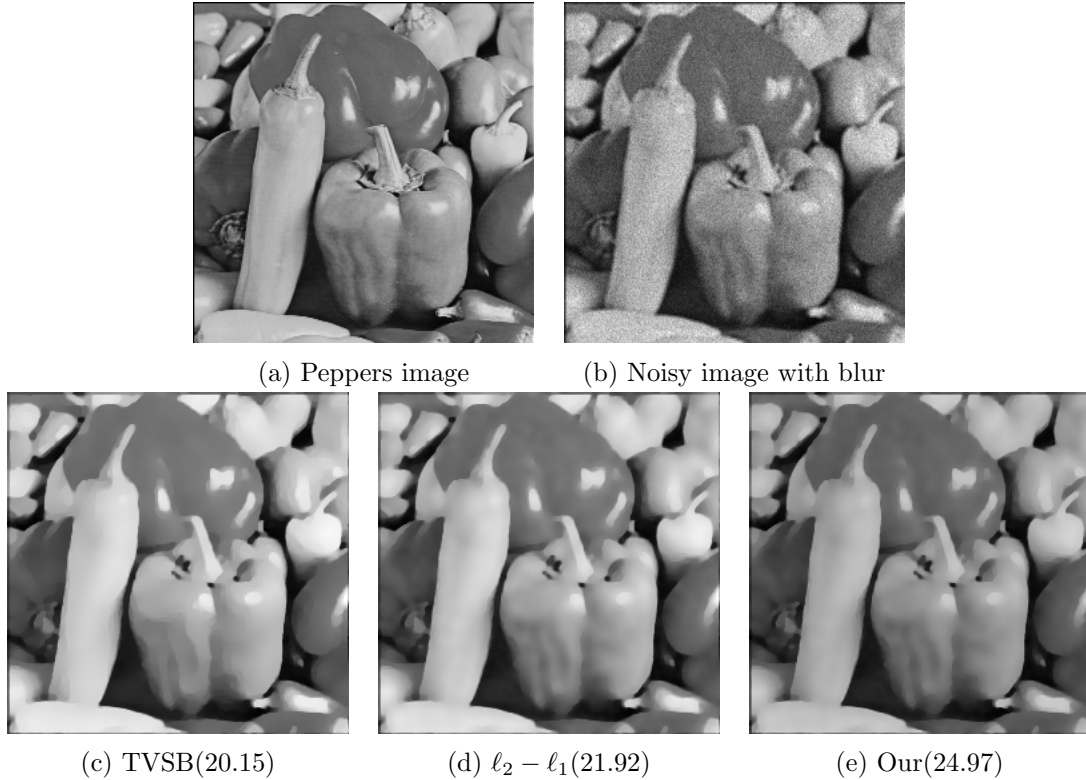


Figure 9: Comparison of denoising results of our model on Peppers image with Gaussian blur with and Poisson noise. PSNR values are reported in bracket.

References

- [1] P. Perona, J. Malik, Scale-space and edge detection using anisotropic diffusion, *IEEE Transactions on Pattern Analysis and Machine Intelligence*, vol. 12(7), pp. 629-639, 1990.
- [2] L. I. Rudin, S. Osher and E. Fatemi, *Nonlinear total variation based noise removal algorithms*, *Physica D: Nonlinear Phenomena*, vol. 60(1), pp. 259-269, 1992.
- [3] M. Lysaker, A. Lundervold, and X.C. Tai, *Noise removal using fourth-order partial differential equation with applications to medical magnetic resonance images in space and time*, *IEEE Trans. Image Process*, vol. 12(12), pp. 1579-1590, 2003.
- [4] K. Papafitsoros, C.B. Schoenlieb, B. Sengul, *Combined first and second order total variation inpainting using split Bregman*, *Image Processing*, vol. 3, pp. 112-136, 2013.
- [5] A. Halim, B.V.R. Kumar, *A $TV - L^2 - H^{-1}$ PDE model for effective denoising*, *Computers and Mathematics with Applications*, vol. 80(10), pp. 2176-2193, 2020.
- [6] T. Le, R. Chartrand, T. Asaki, *A variational approach to constructing images corrupted by Poisson noise*, *J. Math. Imaging Vision* 27 (2007) 257-263.
- [7] S. Setzer, G. Steidl, T. Teuber, *Deblurring Poissonian images by split Bregman techniques*, *J. Vis. Commun. Image Represent.* vol. 2, pp. 193-199, 2010.
- [8] X. Liu and L. Huang, *Total bounded variation-based Poissonian images recovery by split Bregman iteration*, *Math. Methods Appl. Sci.*, 35 (2012), 520-529.

- [9] T. Goldstein, S. Osher, The split Bregman method for L1 regularized problems, *SIAM Journal on Imaging Sciences*, vol. 2(2), pp. 323–343, 2009.
- [10] Xinwu Liu, Augmented Lagrangian method for total generalized variation based Poissonian image restoration, *Computers and Mathematics with Applications*, Vol. 71(8), pp. 1694–1705, 2016.
- [11] D. Li, X. Liu, Anisotropic total generalized variation model for Poisson noise removal, *Multimedia Tools and Applications*, vol. 82(13), pp. 19607–19620, 2023.
- [12] M.R. Chowdhury, J. Qin, Y. Lou Y, Non-blind and blind deconvolution under Poisson noise using fractional-order total variation, *J. Math Imaging Vision*, vol. 62(9), pp. 1238–1255, 2020.
- [13] M.R. Chowdhury, J. Zhang, J. Qin and Y. Lou, *Poisson image denoising based on fractional-order total variation*, *Inverse Problems and Imaging*, vol. 14(1), pp. 77–96, 2020.
- [14] X. Cai, R. Chan, and T. Zeng, *A Two-Stage Image Segmentation Method Using a Convex Variant of the Mumford–Shah Model and Thresholding*, *SIAM Journal of Imaging Sciences*, vol. 6(1), pp. 368–390, 2013.
- [15] R. Chan, H. Yang and T. Zeng, *A Two-Stage Image Segmentation Method for Blurry Images with Poisson or Multiplicative Gamma Noise*, *SIAM Journal of Imaging Sciences*, vol. 7(1), pp. 98–127, 2014.
- [16] T. Wu, J. Shao, X. Gu, M.K. Ng, T. Zeng, Two-stage image segmentation based on nonconvex $l_2 - l_p$ approximation and thresholding, *Applied Mathematics and Computation*, vol. 403, 2021.
- [17] Xinwu Liu, *Augmented Lagrangian method for TV – $l_1 - l_2$ based colour image restoration*, *Journal of Computational and Applied Mathematics*, vol. 354, pp. 507–519, 2019.
- [18] C.T. Pham and T. Tran, An algorithm for hybrid regularizers based image restoration with Poisson noise, *Kybernetika*, vol. 57, 2021.
- [19] D. Mumford, J. Shah, 'Optimal approximation by piecewise smooth functions and associated variational problems', *Commun. Pure Appl. Math*, 1989, Vol. 42, pp. 577–685.
- [20] Z. Wang, A. C. Bovik, H. R. Sheikh, and E. P. Simoncelli, *Image quality assessment: from error visibility to structural similarity*, *IEEE Transactions on Image Processing*, vol. 13(4), pp. 600–612, 2004.